ACS APPLIED MATERIALS & INTERFACES

Research Article

www.acsami.org

Chemical Functionalization of Graphene To Augment Stem Cell Osteogenesis and Inhibit Biofilm Formation on Polymer Composites for Orthopedic Applications

Sachin Kumar,[†] Shammy Raj,[†] Elayaraja Kolanthai,[†] A.K. Sood,[‡] S. Sampath,[§] and Kaushik Chatterjee*[,†]

[†]Department of Materials Engineering, [‡]Department of Physics, and [§]Department of Inorganic and Physical Chemistry, Indian Institute of Science, Bangalore 560012 India

ABSTRACT: Toward designing the next generation of resorbable biomaterials for orthopedic applications, we studied poly(ε-caprolactone) (PCL) composites containing graphene. The role, if any, of the functionalization of graphene on mechanical properties, stem cell response, and biofilm formation was systematically evaluated. PCL composites of graphene oxide (GO), reduced GO (RGO), and amine-functionalized GO (AGO) were prepared at different filler contents (1%, 3%, and 5%). Although the addition of the nanoparticles to PCL markedly increased the storage modulus, this increase was largest for GO followed by AGO and RGO. In vitro cell studies revealed that the AGO and GO particles significantly increased human mesenchymal stem cell proliferation. AGO was most effective in augmenting stem cell osteogenesis leading to mineralization. Bacterial studies revealed that interaction with functionalized GO induced bacterial cell death because of membrane damage, which was further accentuated by amine groups in AGO. As a result, AGO composites were best at inhibiting biofilm formation. The synergistic effect of oxygen containing functional groups and amine groups on AGO imparts the optimal combination of improved modulus, favorable stem cell response, and biofilm inhibition in AGO-reinforced composites desired for orthopedic applications. This work elucidates the importance of chemical functionalization of graphene in polymer composites for biomedical applications.

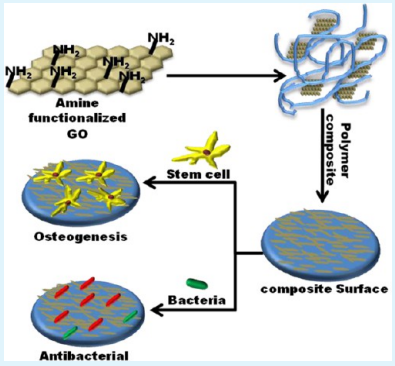

KEYWORDS: *graphene, polymer composites, stem cell, antimicrobial properties, orthopedics*

1. INTRODUCTION

Because of its extraordinary mechanical, thermal and electrical properties graphene is finding increasing use as filler in polymer nanocomposites.[1−3] Graphene-based polymer composites are also being developed for potential use in biomedical applications. Increased conductivity of the graphene composites can be utilized for biosensing. Soft biomedical polymers can be strengthened by incorporating graphene in the polymer matrix for use in hard tissue applications such as orthopedic repair and regeneration in the form of fracture fixation devices, tissue scaffolds, etc. In addition, graphene-derived nanomaterials may be incorporated in composites as a contrast agent to facilitate imaging in vivo.

Good dispersion and strong interfacial interactions between the nanoparticles and the polymer matrix are critical to engineering a strong composite. Graphene is an atomically thin sheet of sp^2 bonded carbon atoms. Good dispersion of such hydrophobic fillers in polymer matrix is a processing challenge. Surfactants are widely used to enhance dispersion but cytotoxicity of many surfactants limits their use in biomedical applications.[4] Chemical functionalization of the surface of the nanoparticles is another popular strategy to increase interactions with the polymer chains of the matrix.[5]

Chemical functionalization of nanoparticles significantly influences the biological response to the particles.[6−8] Molday et al. have shown that functionalization of iron oxide nanoparticles with dextran created more hydroxyl groups on nanoparticle surface, which results in better dispersion stability and binding of amino groups of proteins.[9] Sanpui et al. showed chitosan stabilized silver nanoparticles resulted in severe reduction in viability for human colon cancer cells at very low concentration in comparison to uncoated silver nanoparticles, attributed to well distributed nanoparticles which provided high surface area and access to cell.[10] Bharali et al. reported that amine functionalized silica nanoparticles can be used as effective nonviral vector for gene therapy.[7] Also, it has been reported that amino acid functionalized carbon nanotubes showed enhanced antibacterial activity.[8]

Graphene oxide (GO) is a widely studied form of graphene rich in oxygen, containing functional groups, such as epoxide, carboxyl, and hydroxyl groups.[11] The functional groups of GO can be reduced, thermally or chemically, to yield reduced GO (RGO). Functionalized GO sheets show effective enhancement in mechanical properties of the composites because of better dispersion and interaction with the polymer matrix in comparison to nonfunctionalized graphene sheets.[5]

With the growing interest in the use of graphene for biomedical applications, a number of studies have reported on

Received: November 14, 2014
Accepted: January 13, 2015
Published: January 13, 2015

DOI: 10.1021/am5079732
ACS Appl. Mater. Interfaces 2015, 7, 3237−3252

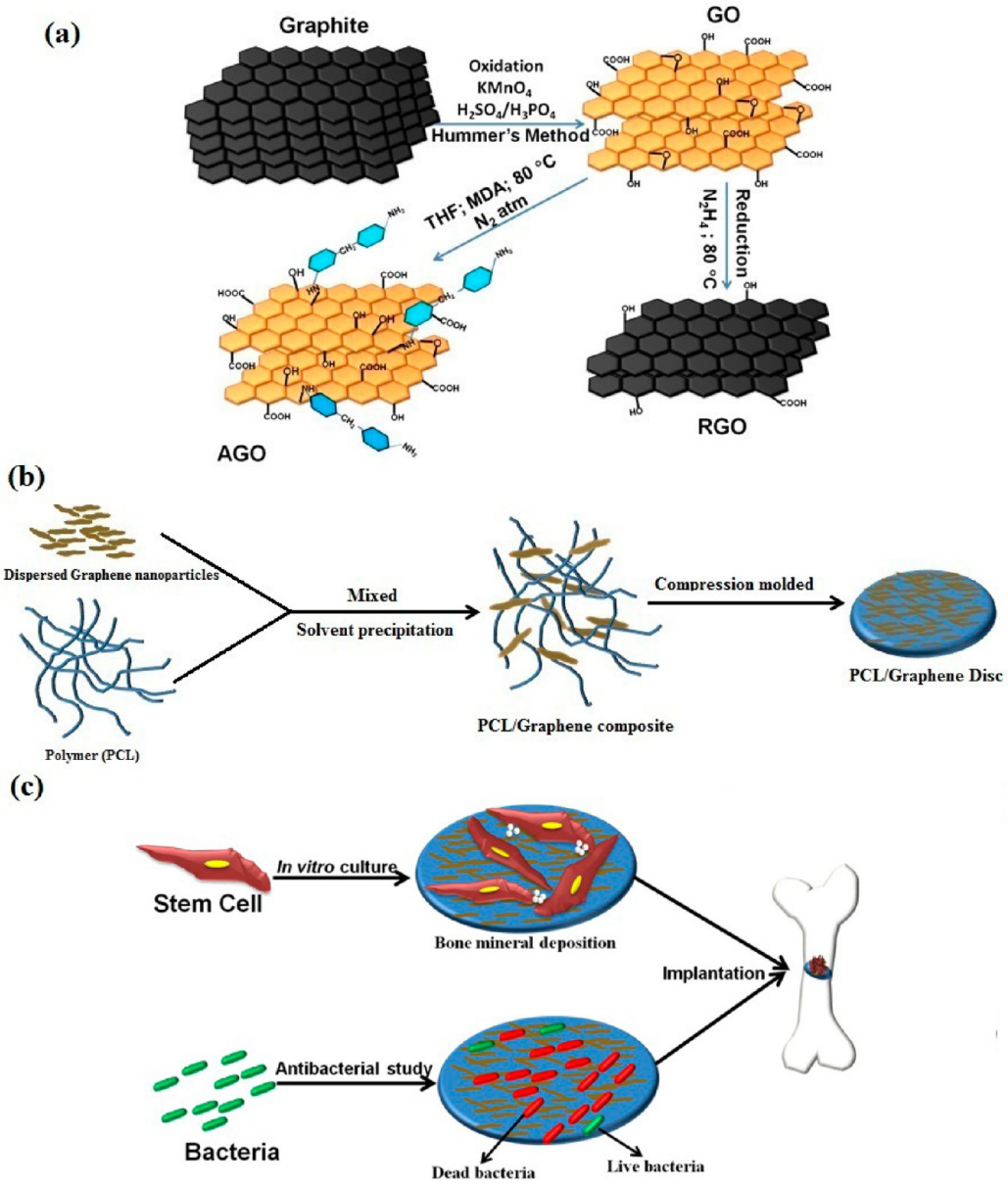

Figure 1. Schematic representation of (a) synthesis of graphene derived nanoparticles (GO, RGO, and AGO), (b) preparation of PCL/graphene composites, and (c) study of stem cell and bacterial response to PCL/graphene composites for orthopedic use.

the interactions with mammalian cells to evaluate its cytotoxicity. Graphene derived nanoparticles have been demonstrated to be biocompatible and also have been tested for drug delivery applications.[12,13] Biocompatibility of graphene nanoparticles are generally achieved by appropriate chemical functionalization of graphene.[14] The surface active groups of GO enhance interaction with proteins thereby helping in cell adhesion and proliferation.[15] On the other hand, hydrophobic RGO impart high electrical conductivity to a surface that has been shown to enhance neural growth.[16] Interestingly both GO and RGO have shown antibacterial property.[17] However, some studies have also reported on the cytotoxicity and mutagenesis induced by graphene.[18]

Recently, graphene-polymer composites have been evaluated for orthopedic applications.[19,20] GO in chitosan matrix was shown to influence cell-scaffold interactions resulting in enhanced osteoblasts proliferation.[19] As a resorbable orthopedic biomaterial, graphene-polymer composites must exhibit good mechanical properties and promote osteogenic differentiation of stem/progenitor cells. Stem cell differentiation and maintenance of pluripotency are largely influenced by cues from the microenvironment.[21] Hence, for stem cell-based tissue engineering, it is imperative to control the physical and chemical properties of the material to guide the fate of the stem cell. In addition, ability to resist attachment and/or growth of bacterial cells that may lead to infections is highly desired. A number of studies have shown that chemistry of the biomaterial surface profoundly influences the response of mammalian and bacterial cells.[22,23] As a result, designing strong composites with appropriate chemical functional groups that actively induce the desired biological response is critical to developing the next generation of bioactive implants. Interestingly, a few reports have demonstrated that biomaterial surface with multifunctional chemical groups (chemical heterogeneity) offer exceptional hemocompatibility and cytocompatibilty.[24,25] Fabrication of biomaterials with surface chemical heterogeneity could influence

DOI: 10.1021/am5079732
ACS Appl. Mater. Interfaces 2015, 7, 3237−3252

the physical, chemical and biological properties because of synergetic effect of different chemical functional groups.

Thus, the aim of this study was to fabricate and characterize mechanical properties and biological response to functionalized graphene nanoparticles in polymer composites. We hypothesized that the presence of different surface chemical moieties on graphene will enhance mechanical properties and influence biological response to the polymeric graphene nanocomposites including both stem cell osteogenesis and bactericidal activity. In this study, we have prepared polycaprolactone (PCL) composites using RGO, GO, and amine-functionalized GO (AGO) at different filler content. PCL is a synthetic biodegradable polyester extensively used in biomedical applications.[26] Mechanical properties of the composites were characterized under dynamic loading. Cellular activity on the composites was assessed by characterizing stem cell proliferation and osteogenic differentiation. Bacterial interactions were assessed by measuring bactericidal activity and biofilm formation.

2. MATERIALS AND METHODS

2.1. Preparation of GO, RGO, and AGO Nanoparticles. Figure 1a schematically presents the synthesis of graphene derived nanoparticles. GO was synthesized by chemical oxidation of natural graphite (Gr) flakes following Hummers method.[27] Briefly, 1.0 g of graphite powder (Superior Company, India) was placed in a flask containing 62 mL mixture of sulfuric acid and phosphoric acid (55:7, Merck) and stirred for 30 min in ice bath. Potassium permanganate (6.0 g, Merck) was added to the flask and stirred at 25 °C for 3 days for oxidation of graphite. Hydrogen peroxide (Thomas Baker, India) was added to stop the reaction and to remove excess potassium permanganate. The graphitic oxide formed was washed with 1 M hydrochloric acid (SDFCL, India) and repeatedly rinsed with deionized water. GO was obtained after centrifugation at 10 000 rpm for 1 h, and dried at 25 °C for 3 days and subsequently in a vacuum oven at 40 °C for 7 days.

RGO was prepared from GO by chemical reduction method using hydrazine hydrate (2 mL per 100 mL of 0.5 mg/mL GO suspension) as reducing agent.[28] To synthesize AGO,[29] 100 mg of GO was dispersed in 40 mL tetrahydrofuran (THF, SDFCL, India) using a bath sonicater (S.V Scientific, India). 250 mg methylene dianiline (MDA, Sigma) was added to the GO solution. The reaction mixture was stirred and refluxed at 80 °C under N_2 atmosphere for 6 h. The product was filtered, washed with ethanol and vacuum-dried at 40 °C for 2 days.

2.2. Characterization of GO, RGO, and AGO. Fourier transform infrared spectroscopy (FTIR, PerkinElmer Frontier IR/NIR systems, USA) from 4000−650 cm^{-1} was used to characterize the synthesized GO, RGO, and AGO. The X-ray diffraction (XPERTPro, PANalytical, UK) patterns of graphene derived nanoparticles were obtained using a Cu Kα radiation source (λ= 1.5406 Å, 40 kV, and 20 mA) with 2θ range of 5° to 60°. Raman spectroscopy (WITEC Raman spectrometer, Germany) of the GO, RGO, and AGO particles was performed using a 514 nm wavelength laser as optical source for excitation. The chemical composition of GO, RGO, and AGO nanoparticles was evaluated using X-ray photoelectron spectrometer (XPS, PHI 1257, PerkinElmer, USA). To analyze surface morphology of graphene derived nanoparticles, GO, RGO, and AGO were dispersed in THF, chloroform and dioxane, respectively, using a bath sonicator. Dispersed graphene nanoparticles were drop casted on a silicon wafer and dried in vacuum for atomic force microscopy (AFM, NanoWizardR 3, JPK Instruments) and scanning electron microscope (SEM, FEI Sirion, USA). Dynamic light scattering (DLS, Zetasizer Nano ZS90, U.K.) was used to analyze average particle size of GO, RGO, and AGO in dispersed state using the standard spherical particle model.

2.3. Preparation of Nanocomposites. PCL/Graphene composites were prepared by solvent precipitation technique as shown schematically in Figure 1b. GO, RGO and AGO nanoparticles were dispersed in THF, chloroform and dioxane, respectively, using bath sonication. PCL (Sigma; $M_n = 8 \times 10^4$) was dissolved at 0.1 g/mL for above-mentioned dispersed graphene nanoparticles in respective solvent. The weight fraction of nanoparticles was varied from 1 to 5 wt % of the polymer. These composites are hereafter designated as PCL/GO_X, PCL/RGO_X, and PCL/AGO_X, wherein X represents the weight fraction (wt %) of the respective graphene nanoparticles. The PCL/GO, PCL/RGO, and PCL/AGO composites were precipitated from the solution in methanol and vacuum-dried at 25 °C for 2 days. Dried precipitated composites were compressed molded into circular discs (5 mm diameter × 0.5 mm height).

2.4. Characterization of PCL/Graphene Composites. The surfaces of PCL and PCL/graphene nanocomposites were imaged using SEM. Thin films of compressed molded samples were placed on aluminum stub and gold-coated before imaging. X-ray diffraction pattern of the samples were recorded at room temperature with 2θ ranging from 5° to 50°. Surface water wettability of the composites was measured using a video-based optical contact angle goniometer (OCA 15EC, Dataphysics, USA) for a 2 μL drop of ultrapure water (Sartorius, Germany). The contact angles reported correspond to mean ± standard deviation (S.D.) for at least three different measurements.

The storage modulus of the PCL and its different PCL/graphene nanocomposites were measured using dynamic mechanical analysis (DMA) (TA Instruments Q800, USA). Rectangular films (length × width × thickness = 15 mm × 5 mm × 0.5 mm) were tested using film tension clamp. Initially a strain sweep was performed on a rectangular sample at 1 Hz to determine critical strain (%) and its respective amplitude was found to be 15 μm which was in linear region of viscoelasticity. Isothermal frequency sweep from 0.1 to 100 Hz at amplitude of 15 μm and a preload of 0.01 N was used at 25 °C.

2.5. Cell Studies. Primary bone-marrow derived human mesenchymal stem cells (hMSCs) from a 25 year old male patient (Stempeutics, India) were cultured in Knockout Dulbecco's modified Eagle medium (DMEM, Invitrogen) supplemented with 15 vol % MSC-qualified fetal bovine serum (FBS, Gibco), 1% glutamax, and 1% antibiotic mixture of penicillin−streptomycin (Sigma). The culture was incubated at 37 °C under 5% CO_2 atmosphere. The culture media was replaced every 3 days until cells reached 70−80% confluency. Cells were removed using 0.25% trypsin (Gibco) and successively subcultured. Prior to seeding cells, composite discs placed in 96-well polypropylene plates (Sigma, nonsurface treated to minimize cell attachment to the plates) were sterilized with 70% ethanol for 30 min and UV exposure for 30 min. Two thousand five hundred cells were seeded in each well containing 200 μL of complete culture media and cultured as described above.

2.5.1. Cell Proliferation and Morphology. Figure 1c schematically summarizes the study of stem cells and bacterial response to the PCL/graphene composites for orthopedic use. hMSC attachment, morphology and proliferation on composites surface were studied using a combination of DNA quantification assay and fluorescence imaging. For DNA quantification, cells on the disc were lysed using 200 μL lysis solution (0.2 mg/mL proteinase K and 0.02% sodium dodecyl sulfate). Picogreen assay (Invitrogen) was used for DNA quantification. Picogreen dye solution (100 μL) was added to equal volume of cell lysate solution. Fluorescence intensity of the solution was measured at 485 nm excitation and 528 nm emission using a microplate reader (Biotek, USA). For fluorescence imaging, hMSCs were fixed on composites surface with 3.7% formaldehyde solution for 30 min and 0.2% TritonX-100 (Sigma) was added to permeabilize cells. The actin filaments and nucleus were stained with 6.6 μM Alexa Fluor 546 (Invitrogen) for 1 h and 14.3 mM DAPI for 15 min, respectively. The stained cells were imaged using an inverted epi-fluorescence microscope (Olympus IX-71). ImageJ software was used to evaluate cell morphology. Outline of the cells was created to measure cell area and the aspect ratio was calculated by fitting an ellipse.

2.5.2. Osteogenic Differentiation. To evaluate the effect of PCL composites reinforced with different chemically functionalized graphene derived nanoparticles on osteogenic differentiation, hMSCs were cultured on the discs in complete culture medium supplemented with known osteoinductive factors (20 mM β glycerophosphate, 10 nM dexamethasone, and 50 μM ascorbic acid, all sourced from Sigma). In vitro mineralization was analyzed by quantifying the calcium deposition

DOI: 10.1021/am5079732
ACS Appl. Mater. Interfaces 2015, 7, 3237−3252

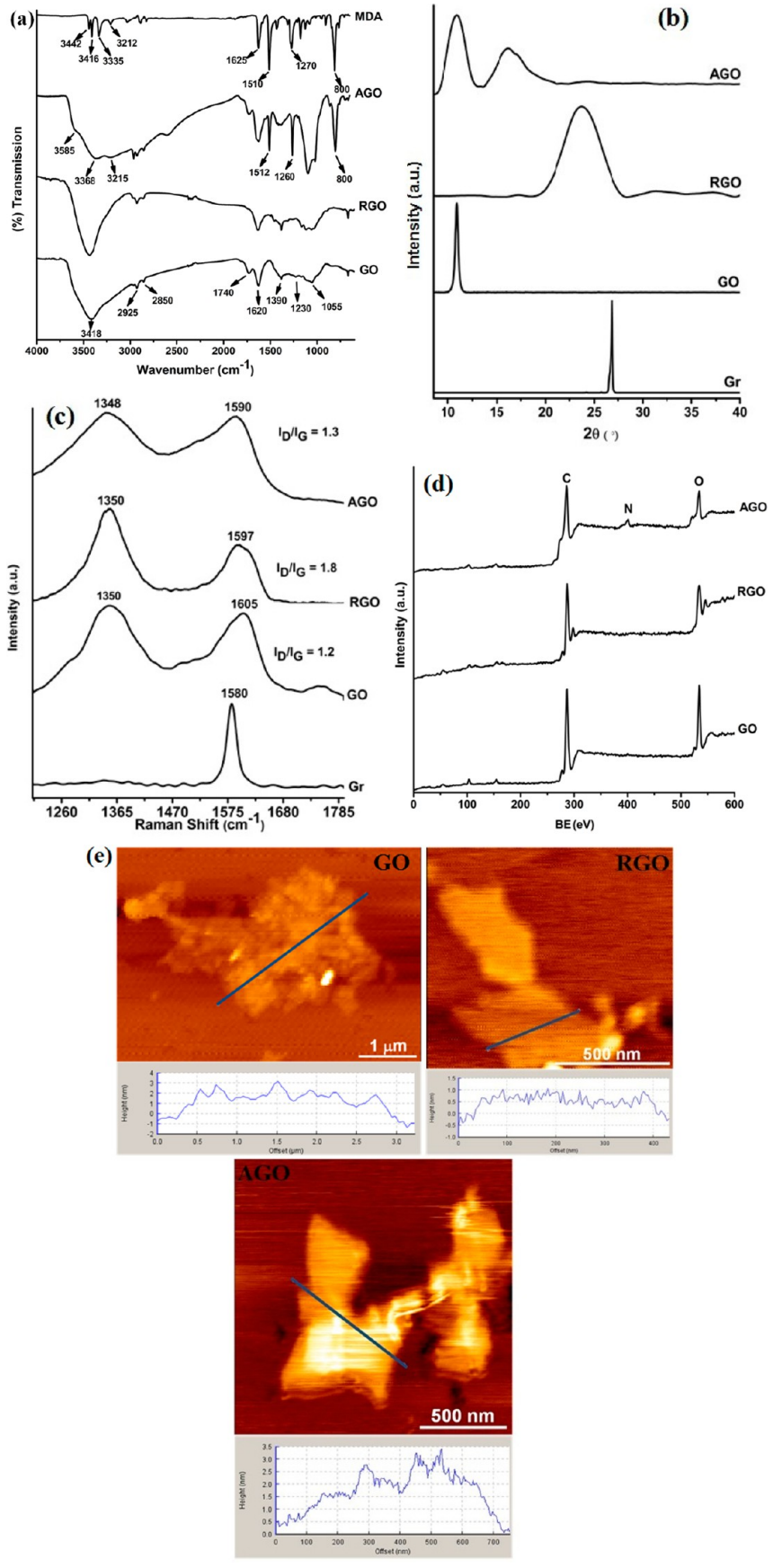

Figure 2. continued

DOI: 10.1021/am5079732
ACS Appl. Mater. Interfaces 2015, 7, 3237−3252

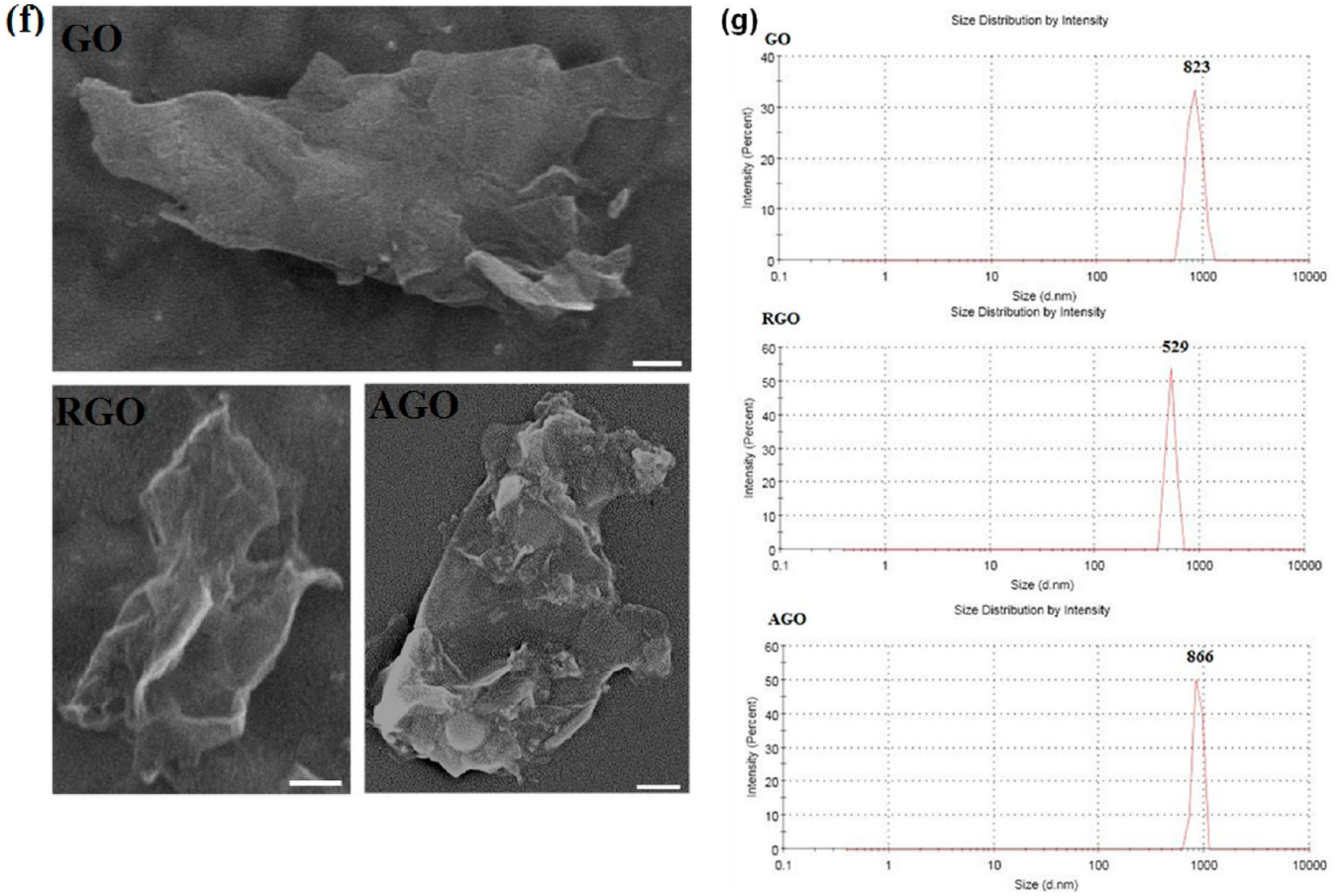

Figure 2. Characterization of graphene derived nanoparticles. (a) FTIR spectra of synthesized GO, RGO, and AGO. (b) XRD profile of Gr, GO, RGO and AGO. (c) Raman spectra for Gr, GO, RGO, and AGO. (d) XPS analysis of GO, RGO, and AGO. (e) AFM images and height profiles of dispersed GO, RGO, and AGO. (f) SEM micrographs of dispersed GO, RGO, and AGO flakes. (g) Size distibution of GO, RGO, and AGO by DLS.

at 14 and 21 days using a previously reported method.[30] Briefly, cells were fixed with 3.7% formaldehyde solution and stained with 2% Alizarin red S (ARS, Sigma) dye. For quantification, the ARS stain was dissolved in 0.2 mL of 5% SDS in 0.5 N HCL for 30 min and absorbance of the solubilized stain was measured at 405 nm using a microplate reader. The chemical nature of mineral deposits was further substantiated by XRD, SEM coupled with energy dispersive X-ray (EDX) and ATR-FTIR.

2.6. Bactericidal Activity and Biofilm Formation. Neat PCL, PCL/GO_5, PCL/RGO_5, and PCL/AGO_5 discs were used to characterize bactericidal nature of these composites by plate counting method.[31] *Escherichia coli* (MG 1655) was grown in 100 mL of sterile Luria Broth (LB) overnight at 200 rpm and 37 °C. 0.5 mL of bacterial suspension adjusted to an optical density (OD) of 0.5 at 600 nm was added to 48 well polystyrene plate containing the sterilized discs. The suspended bacteria were allowed to contact with the sample surface for 2 h at 37 °C. The suspension was removed and the disc surface was washed with 0.9% saline solution. The discs were removed and placed into centrifuge tubes containing 10 mL of 0.9% sterile saline solution. The tubes were bath sonicated for 5 min to remove adhered *E. coli* from the disc surface; 0.2 mL of the diluted bacterial suspension was spread on LB agar plates and incubated at 37 °C for 24 h for colony count. Three plates were used for each sample. *E. coli* colonies grown on agar plate were photographed and the number of viable bacterial colonies was counted. To image adherent bacterial cells on disc surface, the bacterial cells on the surface were washed with saline solution and fixed with 2.5% glutaraldehyde for 30 min. The samples were mounted and gold sputtered prior to SEM imaging.

For viability assay, 0.5 mL of bacterial suspension was allowed to attach to the samples for 2 h as mentioned above. Discs were washed with saline solution twice. Bacterial cells were stained with 100 μL of bacterial live/dead viable stain (BacLight, Invitrogen). The viable stain was prepared by adding 1.5 μL of each dye (SYTO 9 and propidium iodide) in 1 mL of ultra pure water. The stained samples were incubated at ambient temperature for 15 min and then imaged using inverted epi-fluorescence microscope. Live bacteria appear green whereas dead bacterial cells appear red.

To determine the role of reinforced graphene derived nanoparticles on biofilm formation, sterile disc of neat PCL and its composites were placed in 96 well plates and 100 μL of *E. coli* cell suspension (0.5 OD) was added to each well. The plates were incubated for 12 h at 37 °C. After incubation, discs were washed with ultra pure water to remove non-adherent *E. coli*. Attached bacterial cells were fixed using 3.7% formaldehyde solution and observed by SEM for biofilm formation.

2.7. Statistical Analysis. Significant differences between the groups were analyzed using 1-way ANOVA (analysis of variance) with Tukey's test for multiple comparisons used for statistical analysis. Differences were considered statistically significant for $p < 0.05$ and indicated by symbols in figure.

3. RESULTS AND DISCUSSION

3.1. Synthesis and Characterization of GO, RGO, and AGO. The use of Hummers method to prepare GO eliminates the need for metal catalysts in contrast to techniques such as chemical vapor deposition. The presence of metallic catalysts in carbonaceous nanomaterials used in synthesis can induce cytotoxicity.[32] RGO was prepared by chemical reduction of GO,[28] whereas AGO was prepared by grafting MDA through a nucleophilic substitution reaction using oxygenated functional groups of GO as reactive sites.[33]

DOI: 10.1021/am5079732
ACS Appl. Mater. Interfaces 2015, 7, 3237−3252

A variety of independent techniques were used to characterize the synthesized GO, RGO, and AGO nanoparticles. Figure 2a presents FTIR spectra of synthesized GO, RGO and AGO nanoparticles and that of MDA. FTIR spectrum of GO showed peaks at 3418 (O−H stretching), 2925, 2850 (C−H stretching), 1740 (C═O stretching of carboxyl group), and 1620 cm^{-1} (C═C vibration of graphitic domains) and a broad band having peaks at 1390, 1230, and 1055 cm^{-1} representing carboxyl, carbonyl, epoxy, and alkoxy groups, respectively.[28] Presence of these characteristic peaks confirms the existence of oxygen-containing functional groups on GO surface. In contrast to GO, FTIR spectrum of RGO showed narrower peak for O−H stretching at 3435 cm^{-1} and the peaks at 2925 and 2850 cm^{-1} became more intense, whereas peaks at 1740 and 1230 cm^{-1} completely disappeared. Absence of these peaks suggests the reduction of carboxyl and epoxy groups from GO surface by hydrazine hydrate.[28] Furthermore, intense peak at 2925 cm^{-1} in RGO indicates the restoration of sp^2 hybridization.[34] Hence, all observations from FTIR suggest chemical reduction of GO by hydrazine hydrate.

AGO showed FTIR spectra similar to that of GO with broad O−H and doublet N−H stretching peaks at ∼3500, 3368, and 3215 cm^{-1}. In addition, it showed peaks at 1512 (phenyl group of MDA[35]), 1260 (C−N stretching of aryl group), and 800 cm^{-1} (N−H bending). MDA showed peaks at 3442, 3416, 3335 and 3212 cm^{-1}, which corresponds to antisymmetric and symmetric stretching for amine group. It also showed characteristic peaks for N−H bending, C−N aryl stretching and N−H bending loop at 1625, 1270, and 800 cm^{-1}. Further the intense peaks at 1510 cm^{-1} attributed to C−C stretching for aromatic ring. FTIR peaks of AGO closely match with GO and MDA confirming the grafting of MDA moieties onto the GO surface.

Figure 2b shows XRD patterns for Gr, GO, RGO, and AGO. Gr flakes showed diffraction peak at 26.8° corresponding to *d* spacing of ∼3.4 Å. After oxidation, GO flakes showed diffraction peak at 10.9° representing *d* spacing of ∼8.1 Å. This increase in *d* spacing after oxidation is attributed to increase in interlayer distance of oxidized graphite because of the presence of oxygenated functional groups on GO surface.[36] RGO showed a broad peak at 23.7° with an estimated *d* spacing of ∼3.8 Å. The broad XRD peak for RGO suggests an increase in disorder.[37] On the other hand, decrease in *d*-spacing in RGO was because of the chemical reduction of oxygenated functional groups on GO. AGO exhibited two broad diffraction peaks at 10.9° and 16.2°. The broad peak at 10.9° indicates AGO sheets persist in random order,[33] whereas broad peak at 16.2° may be attributed to crystalline nature of MDA.

Figure 2c shows Raman spectra of Gr, GO, RGO, and AGO. Gr flakes showed only G band at 1580 cm^{-1} that corresponds to in plane vibration of sp^2 carbon atom.[38] GO, RGO, and AGO showed not only G (∼1600 cm^{-1}) but also characteristic disorder induced (D) bands at ∼1350 cm^{-1}. The peak area ratios of D band to G band (I_D/I_G) for GO, RGO, and AGO was 1.2, 1.8, and 1.3, respectively. The increase in I_D/I_G value from 1.2 to 1.8 during chemical reduction of GO to RGO is indicative of presence of large number of defects likely due to high density of edges and disorder in graphene layers,[39] corroborated by the broad XRD peak for RGO. The small frequency shift toward lower wavenumber for RGO was observed when compared to GO, which indicates structural change in GO during chemical reduction.[40] However, very broad D and G bands for AGO arise because of the presence of defects on graphene sheet upon amine functionalization.[41] Since AGO and GO nanoparticles showed nearly the same I_D/I_G value (1.3 and 1.2), the number of defects on AGO and GO are similar. It also indicates that the crystallite size for GO and AGO are similar, consistent with the findings of other studies.[41] This is also corroborated by XRD data (peaks at 10.9°) for GO and AGO.

Figure 2d shows XPS spectra of GO, RGO, and AGO nanoparticles. Typically all three graphene derived nanoparticles showed C 1s and O 1s peaks at ∼285 and ∼534 eV, respectively. AGO showed an additional peak at ∼400 eV corresponding to nitrogen peak (N 1s).[33] The elemental quantification for carbon, oxygen, and nitrogen for GO, RGO, and AGO are summarized in Table 1.

Table 1. XPS Elemental Quantification for GO, RGO, and AGO Nanoparticles

particle	carbon (wt %)	oxygen (wt %)	nitrogen (wt %)	C/O (weight ratio)
GO	69	31	0	2.2
RGO	80	20	0	4.0
AGO	57	24	19	2.3

The XPS spectra for RGO showed a decrease in oxygen peak intensity in comparison to GO. The elemental analysis showed that C/O weight ratio for RGO was higher than that of GO. These results indicate the reduction of GO to RGO during reaction by hydrazine. The presence of N 1s peak in XPS spectra for AGO confirmed the existence of amine group on GO surface suggesting effective grafting of MDA on AGO surface. The content of nitrogen on AGO was found to be 19 wt %. Thus, characterization of the synthesized graphene derived nanoparticles using a combination of FTIR, XRD, Raman spectroscopy and XPS techniques confirmed the formation of GO, RGO, and AGO.

Figure 2e shows AFM images of GO, RGO, and AGO nanoparticles in tapping mode. The thickness of GO sheets was ∼2 nm. The thickness of RGO sheets was ∼1 nm and its lateral size was around 500 nm, which is consistent with other report.[16] Amine functionalized GO (AGO) sheets showed slight higher thickness of ∼3 nm. The observed thickness of GO was slightly higher than typical single layer GO sheet[17] (around 1 nm). This may be due to overlap of few GO sheets. The increase in thickness for AGO sheets may be probably due to grafting of MDA on GO surface. Representative SEM micrographs of GO, RGO, and AGO are presented in Figure 2f. SEM micrographs show GO sheets size of around 1 μm and after hydrazine reduction the size of GO sheets reduced to ∼500 nm for RGO. AGO showed similar sheet size to that of GO. Furthermore, the average particle size of GO, RGO, and AGO were characterized by DLS. Figure 2g shows the average size of dispersed GO, RGO, and AGO were 823, 529, and 886 nm, respectively. DLS also confirmed the reduction in the size of GO after chemical reduction. On the other hand, GO and AGO showed similar particle size. As graphene particles are not spherical the particle size determined here may not be accurate. However, DLS provided a relative particle size variation of GO, RGO, and AGO in dispersed state corroborating the trends seen in AFM and SEM.

3.2. Characterization of PCL/Graphene Composites. Preparation of PCL/graphene nanocomposites is shown schematically in Figure 1b. Presence of well dispersed nanoparticles on the surface of polymer matrix plays a key role in influencing the physical, chemical, and biological properties of

DOI: 10.1021/am5079732
ACS Appl. Mater. Interfaces 2015, 7, 3237−3252

the polymer composites. Figure 3a shows surface SEM micrographs of neat PCL, PCL/GO_5, PCL/RGO_5, and

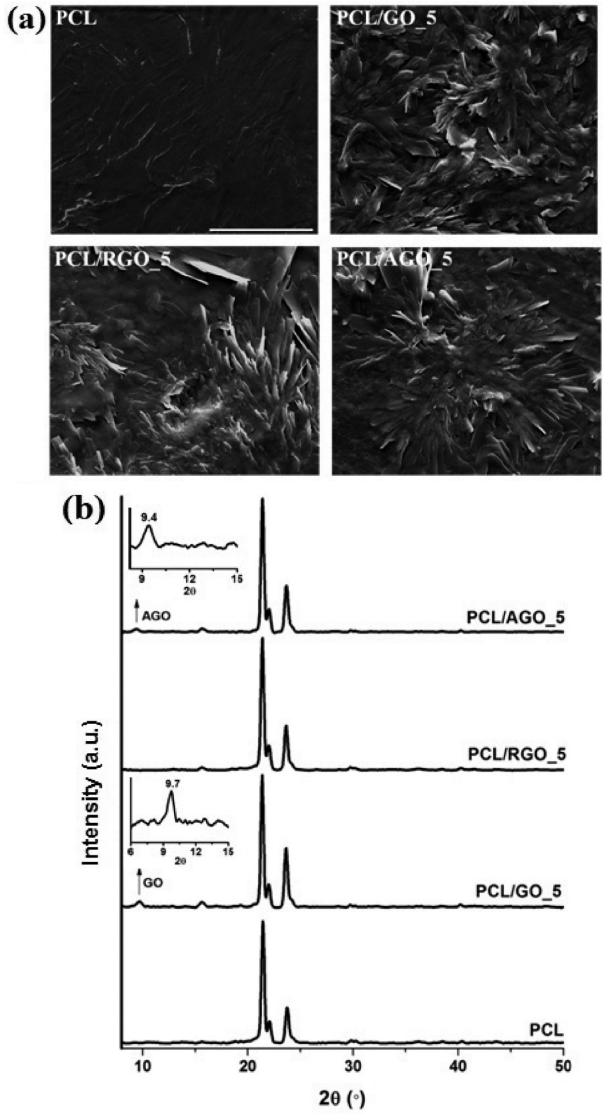

Figure 3. (a) Surface SEM micrographs of neat PCL, PCL/GO_5, PCL/RGO_5, and PCL/AGO_5 composites thin films (scale bar = 20 μm). (b) XRD pattern of neat PCL and its composites film.

PCL/AGO_5 composite thin films. Composites showed presence of embedded strips of the respective graphene sheets on the PCL surface. Increase in the surface roughness of PCL with the addition of nanoparticles is due to the formation of irregular protuberance by the nanoparticles.

Figure 3b represents XRD pattern of neat PCL and its composites film. Neat PCL showed two intense diffraction peaks at 21.3° and 23.6° representing (110) and (200) planes of orthorhombic crystalline form.[42] Moreover PCL/GO_5, PCL/RGO_5, and PCL/AGO_5 showed similar peak positions to that of neat PCL suggesting crystal structure of PCL remained unchanged with addition of GO, RGO, and AGO nanoparticles. In PCL/GO_5 and PCL/AGO_5 composites diffraction peaks of the respective nanoparticles (GO and AGO) were observed at 9.7° and 9.4°, respectively (Figure 3b inset). It further confirms the presence of GO and AGO nanoparticles in PCL matrix. On the other hand, diffraction peak for RGO nanoparticles expected at 23.7° (as shown by XRD Figure 2b) in PCL/RGO_5 composites might have been suppressed by the PCL peak at 23.6°. Also it was observed that with the addition of nanoparticles in PCL matrix peak intensity of (200) plane increased. PCL/GO_5 composites showed highest increase in (200) plane, followed by PCL/AGO_5 and PCL/RGO_5 composites. These results indicate that the addition of graphene derived nanoparticles increased the crystallinity of PCL without affecting its crystal structure.

Figure 4a shows the water wettability of PCL and its composites reinforced with different surface functionalized graphene nanoparticles. With incorporation of GO and AGO nanoparticles wettability of PCL increased, whereas addition of RGO nanoparticles increased the hydrophobicity of PCL. The increase in hydrophilicity of PCL/GO and PCL/AGO composites can be attributed to the presence of hydrophilic functional groups on GO and AGO surface. Chemical functionalization of graphene (GO and AGO) results in increased surface energy of the graphene nanoparticles because of the existence of polar functional groups.[43] Reinforcement of graphene nanoparticles having polar functional groups with high surface energy results in increased wettability of the PCL composite. Addition of RGO nanoparticles, which lack oxygenated functional groups, imparts hydrophobicity to RGO resulting in increased contact angle for PCL/RGO composites.

The storage modulus obtained at a frequency of 1 Hz for three replicates each of neat PCL and the PCL/graphene composites are shown in Figure 4b. It was observed that the storage modulus of PCL increased monotonically with the fraction of graphene in the polymer. The storage modulus of PCL increased from 344 MPa reaching up to 626, 497, and 569 MPa after addition of 5 wt % of GO, RGO, and AGO, respectively. Enhancement in storage modulus of PCL/graphene nanocomposites with graphene reinforcement can be attributed to stress transfer from soft polymer matrix to hard graphene nanoparticles.[44] Presence of structural distortion or defects in graphene sheets reduces strength of graphene, which may result in relatively small improvement in mechanical properties for polymer/graphene composites.[45] As a result, the addition of more defective RGO (I_D/I_G =1.8) (Figure 2c) showed relatively smaller improvement in storage modulus for PCL/RGO composites. In contrast, the presence of less defective GO (I_D/I_G =1.2) and AGO (I_D/I_G =1.3) (Figure 2c) sheets results in better enhancement in storage modulus of PCL with the largest increase observed for GO composites. Moreover, addition of GO nanoparticles in PCL was shown to increase crystallinity of PCL (Figure 3b) thereby further enhancing the modulus of PCL/GO composites.

3.3. Biological Studies. Chemical properties of the surface of biomaterials strongly influence the biological response at material-biology interface, which subsequently control cellular behavior such as attachment, spreading, proliferation, cell signaling and differentiation.[46] Thus, addition of chemical functional groups to graphene particles provides an opportunity to modulate biological responses at the biomaterial interface. Figure 1c schematically shows the study of biological response to PCL/graphene composites. Cell−material interaction was studied by assessing cellular proliferation, morphology and mineralization of primary bone-marrow derived hMSCs. MSCs are multipotential stem cells capable of differentiating into many lineages. Of particular relevance to this study, MSCs can undergo osteogenic differentiation for repair and regeneration of bone tissue. Thus, hMSC response to the different composites is

DOI: 10.1021/am5079732
ACS Appl. Mater. Interfaces 2015, 7, 3237−3252

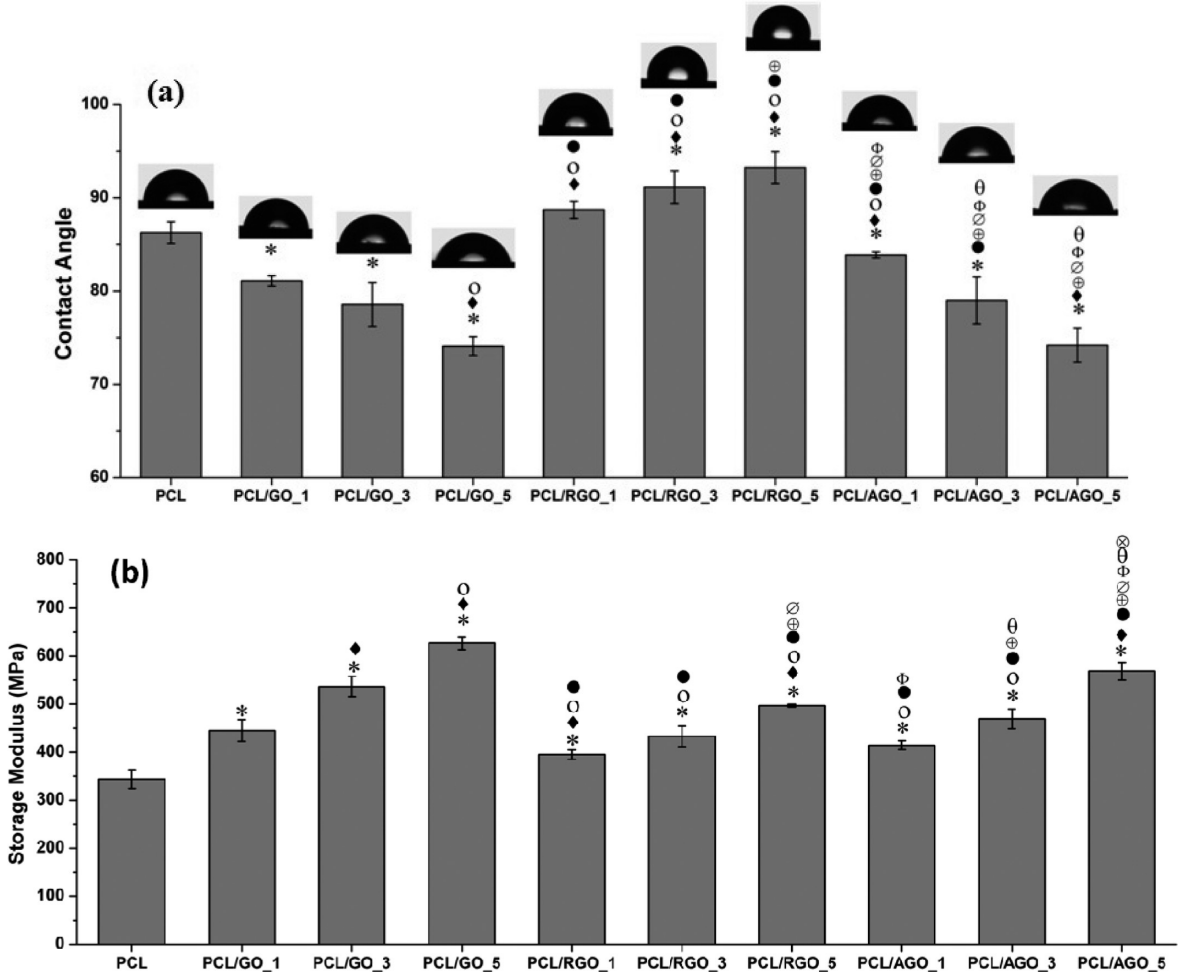

Figure 4. (a) Water contact angle of neat PCL and its different graphene derived composites and (b) DMA analysis of PCL and its composites. Results are represented as mean ± SD for $n = 3$ for both water contact angle and DMA analysis. Statistically significant difference ($p < 0.05$) compared to PCL, PCL/GO_1, PCL/GO_3, PCL/GO_5, PCL/RGO_1, PCL/RGO_3, PCL/RGO_5, PCL/AGO_1, and PCL/AGO_3 are indicated by *, ♦, *o* ●,⊕, ⌀, Φ, *θ*, and ⊗, respectively.

indicative of the potential of these composites for use in orthopedics.

3.3.1. Cell Proliferation. Figure 5a compiles results of DNA quantification at 1 day and 7 days after cell seeding. At day 1, there were no significant differences in DNA content between the PCL and its different composites. The DNA content increased on all the discs with time from 1 to 7 days indicating hMSCs had proliferated well on all the samples. The DNA content was not significantly higher with the addition of 1 wt % of GO to PCL, whereas the addition of 3 and 5 wt % of GO in PCL resulted in significant increases in DNA content with respect to neat PCL. For PCL/RGO composites, reinforcement of 1 and 3 wt % of RGO did not show any significant increase in DNA content. The addition of 5 wt % of RGO in PCL showed significant increase in DNA content in comparison to neat PCL and PCL/GO_1. Interestingly, for PCL/AGO composites, the addition of just 1 wt % of AGO resulted in a significant enhancement in DNA content. As a result, all the three PCL/AGO composites showed significant increase in DNA content when compared to neat PCL, PCL/GO_1 and all the three PCL/RGO composites. Figure 5b shows fluorescence micrographs of stained nuclei of hMSCs at 1 and 7 days. As can be seen from the micrographs, increased numbers of nuclei were seen on all the samples from day 1 to day 7 indicating proliferation of hMSCs on all the samples. These observations support the results of the DNA quantification assay.

Cellular responses to biomaterials are controlled by several properties including both chemical and physical properties from the biomaterial surface. Addition of nanoparticles with different functional groups with different charge and hydrophilicity induces changes in surface chemistry influencing the biological responses.[47] Taken together, the result of DNA quantification assay and fluorescence imaging suggest that all the composites are suitable for attachment and proliferation of hMSCs and are not cytotoxic. These data also suggest that reinforcement of polymer matrix by graphene nanoparticles not only minimizes toxicity of the nanoparticles but also enhances the biological properties the polymer. The presence of the functionalized nanoparticles increased the surface water wettability of the polymer (Figure 4a). Cells attach and proliferate better on hydrophilic surfaces than hydrophobic surfaces. Hydrophilic surfaces mediate the binding of adhesive proteins, such as fibronectin and vitronectin, which can facilitate cell adhesion and growth.[48] Thus, reinforcement of PCL by GO and AGO enhanced cell proliferation because of increased hydrophilicity of the composites in contrast to PCL and the RGO composites. It has been demonstrated that metal surfaces coated with carboxyl, hydroxyl, and amine functional groups help in cell attachment

DOI: 10.1021/am5079732
ACS Appl. Mater. Interfaces 2015, 7, 3237−3252

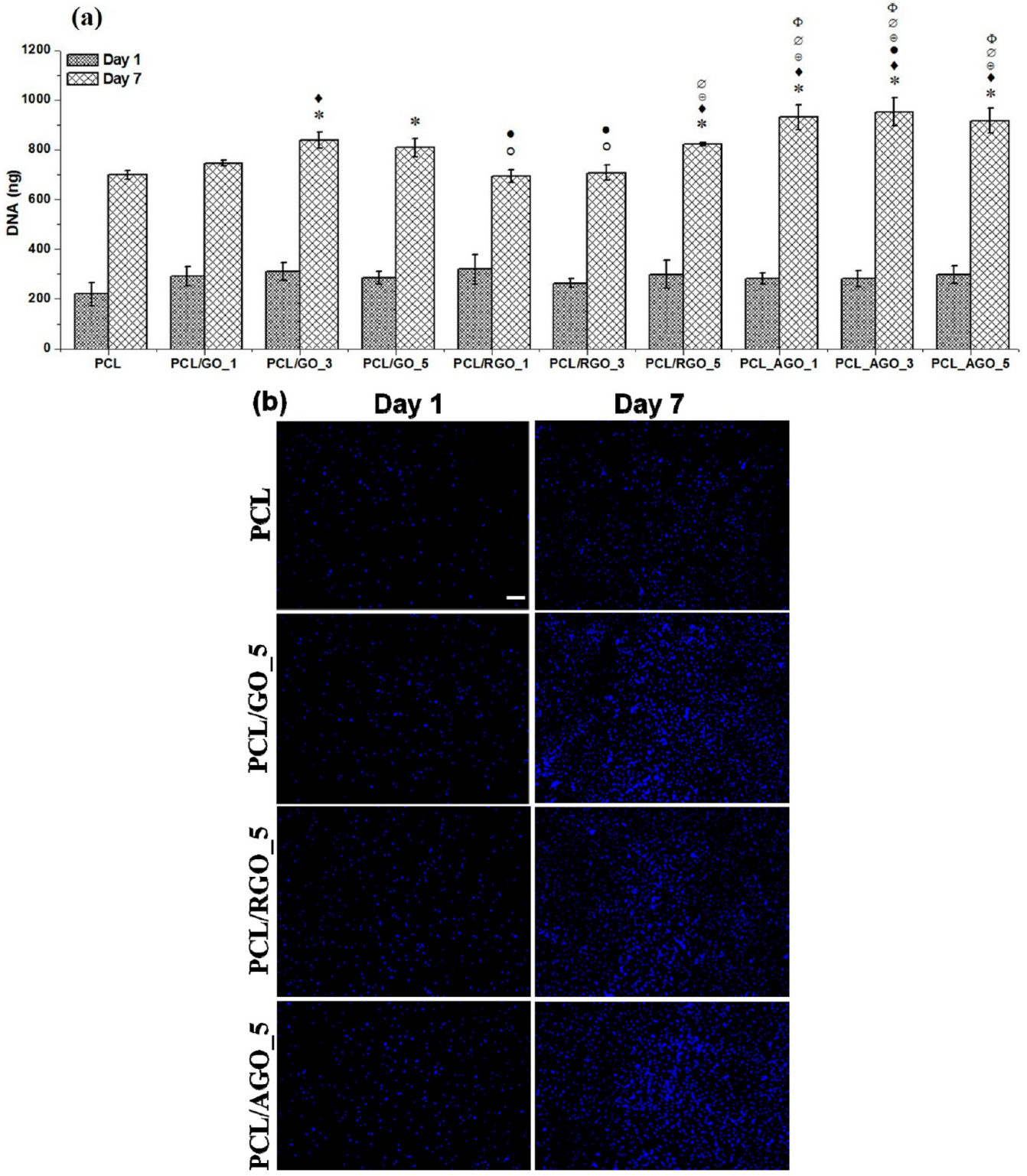

Figure 5. (a) DNA content at 1 and 7 days after cell seeding on PCL and its graphene derived composites. (b) Fluorescence micrographs of stained nuclei of hMSCs 1 and 7 days (scale bar = 0.1 mm). Statistically significant difference ($p < 0.05$) compared to PCL, PCL/GO_1, PCL/GO_3, PCL/GO_5, PCL/RGO_1, PCL/RGO_3, and PCL/RGO_5 are indicated by *, ♦, *o* ●,⊕, ⌀, and Φ respectively.

and proliferation.[49] The presence of AGO in PCL supported marginally higher proliferation than GO nanoparticles likely resulting from favorable adsorption of cell-adhesive proteins by amine nanoparticles.[47,49] Protein adsorption to the more hydrophobic RGO particles is less favorable for cell attachment resulting in less proliferation on PCL/RGO surface. Thus, addition of functionalized graphene nanoparticles with polar, hydrophilic groups influenced the surface chemistry of the composites resulting in better cell attachment and proliferation.

3.3.2. Cell Morphology Analysis. It now well recognized that morphology of a cell is important for its function.[50] Chemical and topographical properties of the biomaterial influence protein

DOI: 10.1021/am5079732
ACS Appl. Mater. Interfaces 2015, 7, 3237−3252

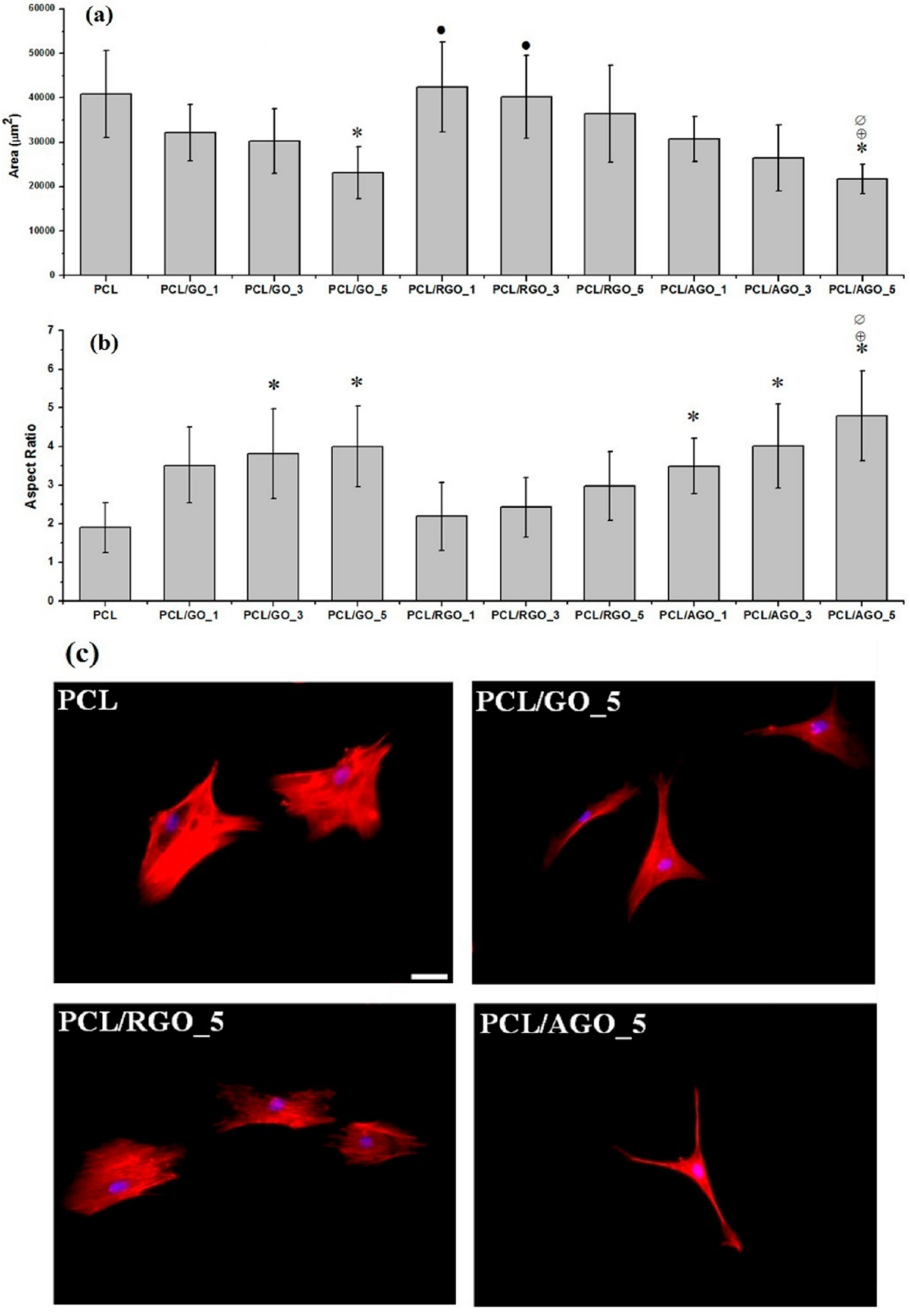

Figure 6. Morphology analysis of hMSCs on PCL and PCL/graphene-derived composites: (a) Area of hMSCs, (b) aspect ratio of hMSCs, (c) representative fluorescence micrographs of hMSCs showing actin filament (red) and nuclei (blue) (scale bar = 40 μm). Statistically significant difference ($p < 0.05$) compared to PCL, PCL/GO_5, PCL/RGO_1 and PCL/RGO_3 are indicated by *, •, ⊕, and ⌀, respectively.

adsorption when seeded with cells in serum-containing media and subsequently regulate cell morphology.[46] Regulation of cell morphology at early time is predictive of the fate of stem cells.[51] Hence, we systematically characterized hMSC morphology on different PCL composites.

hMSCs on the PCL/GO and PCL/AGO surfaces exhibited spindle-shaped, elongated and branched morphology with high

DOI: 10.1021/am5079732
ACS Appl. Mater. Interfaces 2015, 7, 3237−3252

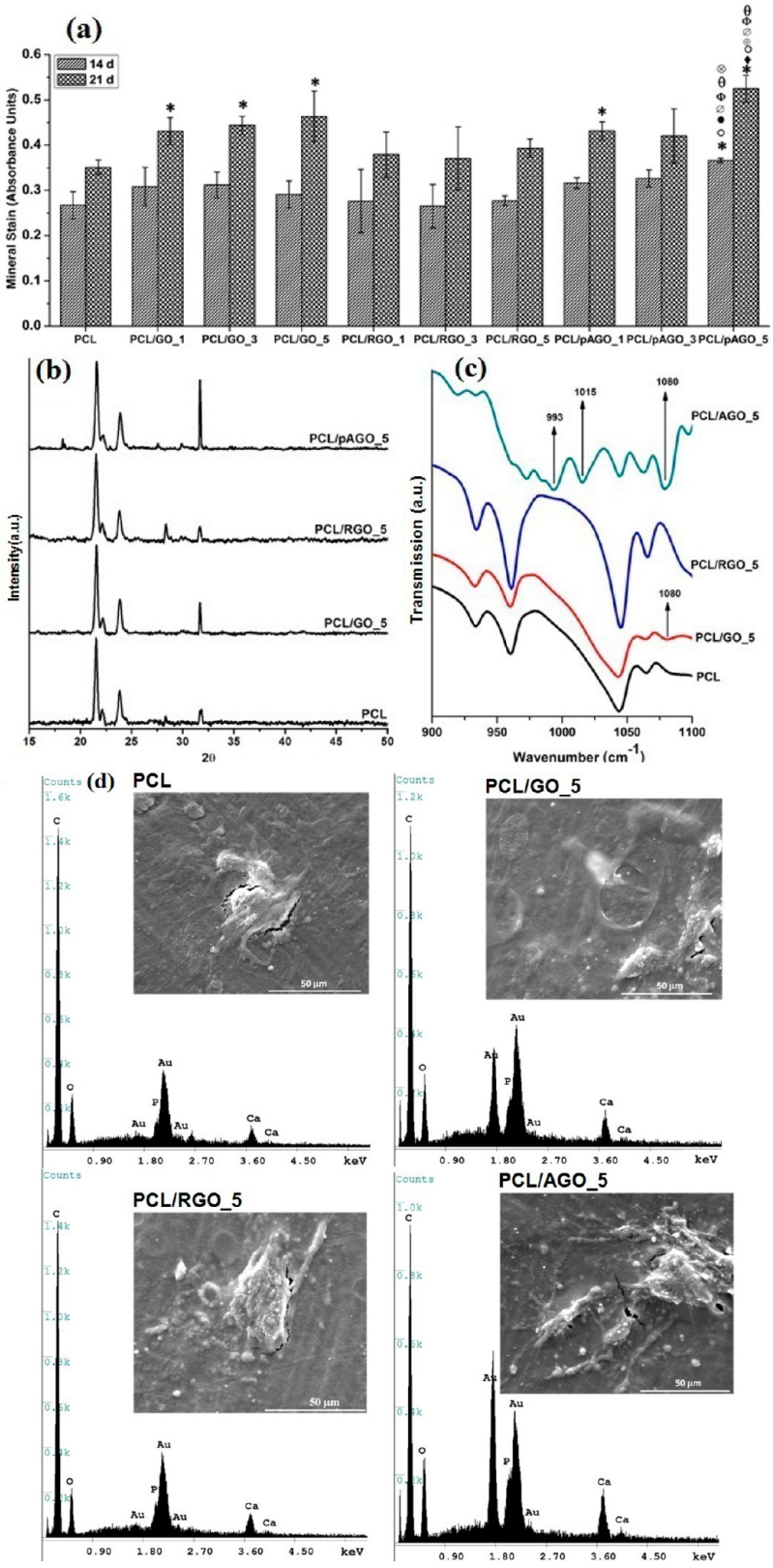

Figure 7. Analysis of mineral deposits by hMSCs(a) quantification on PCL and its different composites at days 14 and 21 using ARS dye. (b) XRD pattern of mineral deposits on PCL, PCL/GO_5, PCL/RGO_5, and PCL/AGO_5. (c) ATR-FTIR spectra for mineralized composites for day 21. (d) SEM micrograph with EDS analysis of mineral deposited composites. Statistically significant difference ($p < 0.05$) compared to neat PCL, PCL/GO_1, PCL/GO_3, PCL/GO_5, PCL/RGO_1, PCL/RGO_3, PCL/RGO_5, PCL/pAGO_1, and PCL/pAGO_3 are indicated by *, ♦, ○, ●,⊕, ⌀, Φ, θ, and ⊗, respectively.

DOI: 10.1021/am5079732
ACS Appl. Mater. Interfaces 2015, 7, 3237−3252

aspect ratio and low spread area (Figure 6). In contrast, cells on PCL/RGO were circular and well spread with significantly higher cell spread area. Similar observation have been observed for osteoblasts which exhibited high aspect ratio and low area on amine functionalized surfaces.[30,46] Presence of highly branched and elongated cells on PCL/GO and PCL/AGO surface was due to the presence of functionalized graphene derived nanoparticles (GO and AGO) in the PCL matrix. Although the hydrophobic RGO particles in PCL did not significantly affect cell attachment as seen in the DNA content assay (Figure 5a), it affected cell morphology yielding rounded cells with larger spread area. Studies have shown that a hydrophilic surface helps in better cell attachment and elongation compared to a hydrophobic surface.[52] Presence of amine functional groups on the surface influence protein adsorption and induces favorable changes in protein conformation.[53] The conformation of the adsorbed proteins on surfaces rich in amine and hydroxyl groups favors more integrin binding in osteoblasts thereby enhancing formation of focal adhesions and ultimately the activation of osteogenic pathways.[54] Therefore, the presence of highly branched and significantly elongated hMSCs on PCL/AGO and PCL/GO surfaces suggested that these surfaces were likely to augment osteogenic differentiation.

3.3.3. Osteogenic Differentiation. Mineral deposition is the final stage of osteogenic differentiation. Figure 7a compiles the quantification of mineral deposited on PCL and its different graphene derived composites at day 14 and 21 using ARS dye. At day 14, only PCL/AGO_5 composite showed significantly higher mineral deposition compared to neat PCL. On day 21, neat PCL and all the three PCL/RGO composites showed nearly the same mineral content. PCL/GO and PCL/AGO composites showed significantly more mineral deposition than neat PCL. The mineral content increased with increase in fraction of GO and AGO in PCL. The mineral deposition on PCL/AGO_5 was highest among all the samples and was 40% higher than on neat PCL. PCL/GO_5 showed ~25% more mineral deposition than neat PCL. Figure 7b shows XRD pattern of mineral deposition of hMSC on PCL composites. XRD profile confirms the formation of hydroxyapatite on mineralized composite surface as revealed by the peak at 31.7°.[55] All the samples showed peaks for hydroxyapatite. But the peak intensity was highest for PCL/AGO_5 composite and followed by PCL/GO_5 and was least for PCL/RGO_5 and PCL. This trend is in good agreement with the mineral content determined by ARS method (Figure 7a). The presence of phosphate groups in the ATR-FTIR was used to further confirm the nature of the mineral deposits. Figure 7c shows FTIR spectra for mineralized composites for day 21. PCL/GO_5 composites showed peak at 1080 cm^{-1} corresponding to phosphate stretching. PCL/AGO_5 composite showed phosphate peaks at 993, 1015, and 1080 cm^{-1}.[30] Interestingly, PCL/AGO_5 composites showed intense and clear peaks for phosphate groups in comparison to neat PCL and all other composites. Figure 7d presents SEM micrographs with EDS analysis of mineral deposited on the composites. SEM micrographs showed characteristic mineralized bone-like nodules deposited by hMSCs on the composites surface (Figure 7d inset). The elemental calcium (Ca) and phosphorus (P) peaks were seen in EDS. Similar to the trends observed with other techniques, intensity of Ca and P peaks for PCL/AGO_5 composite was higher compared to other composites and neat PCL.

In this study, a library of polymer nanocomposites was prepared using graphene with different chemical functionalization to enhance surface bioactivity in addition to improvement in mechanical strength. The bioactivity of composites was assessed by studying mineralization resulting from osteogenesis of hMSCs cultured on the composites. It has been shown that hMSCs when cultured in medium supplemented with osteogenic factors induces osteogenic differentiation and support mineral deposition in the presence of bioactive materials.[56] Quantitative analysis of mineral deposition by hMSC on composites showed increased mineral content from day 14 to day 21 suggesting osteogenic differentiation and subsequently mineralization. XRD profile of the mineralized composite surfaces revealed that mineralized phase deposited by hMSCs as hydroxyapatite. FTIR analysis further supported mineral deposition by showing characteristic phosphate (O−P−O) band present in hydroxyapetite. SEM micrographs and EDS analysis confirmed deposition of mineralized nodules around hMSCs. All these results showed better mineral deposition on PCL/GO and PCL/AGO composites in comparison to neat PCL and PCL/RGO composites. This is likely because the carboxyl and amine functional groups on functionalized graphene serve as binding site for calcium and phosphate ions, as reported earlier.[57,58] Moreover, it has been shown that GO nanoparticles have high affinity to adsorb dexamethasone and β-glycerophosphate, the osteoinductive factors used in this study resulting in increased osteogenic differentiation and mineralization.[15] This would have further facilitated better differentiation and mineralization in the GO composites as compared to the nonfunctionalized RGO nanoparticles. Enhanced hMSC differentiation is reflected by the increased mineral content with increase in GO content in PCL. Also, as we have shown in a recent study, addition of amine-functionalized nanotubes in polymer composites can promote osteoblast proliferation and mineralization.[30] Thus, the addition of AGO particles to PCL containing both amine and carboxyl functional groups (as shown in FTIR Figure 2a) showed better mineralization because of synergetic effect of the functional groups by putatively facilitating the nucleation of hydroxyapatite.[59] Thus, composites having high content of functionalized graphene (PCL/AGO_5 and PCL/GO_5) were influential in driving the stem cells to regulate their metabolic activity toward osteogenic differentiation. Thus, results of osteogenic differentiation and mineralization studies confirmed the highest mineralization on amine functionalized graphene composites (PCL/AGO_5) suggesting the potential use of PCL/AGO composites with multi chemical functionalities for orthopedic applications.

3.4. Antibacterial Test. Bacterial infection associated with implants primarily caused by adhesion and biofilm formation on the biomaterial surface is a major clinical challenge.[60] Bacterial biofilm formation on biomaterials is a complex process and is governed by many factors including the physical and chemical properties of the material, surface properties of bacteria and environmental conditions.[61] Attachment of bacteria on indwelling biomaterial surface prevents the interaction of biomaterials with surrounding biological environment, which limits biological performance of the biomaterials.[62,63] It is important to assess the interaction of bacteria and biomaterials for its optimum clinical performance. Thus, in this study we also analyzed the bactericidal property of PCL/graphene composites. PCL composites with high content (5 wt %) of graphene derived nanoparticles, which exhibited good physical properties and osteogenesis were used to study antibacterial activity against *Escherichia coli*.

DOI: 10.1021/am5079732
ACS Appl. Mater. Interfaces 2015, 7, 3237−3252

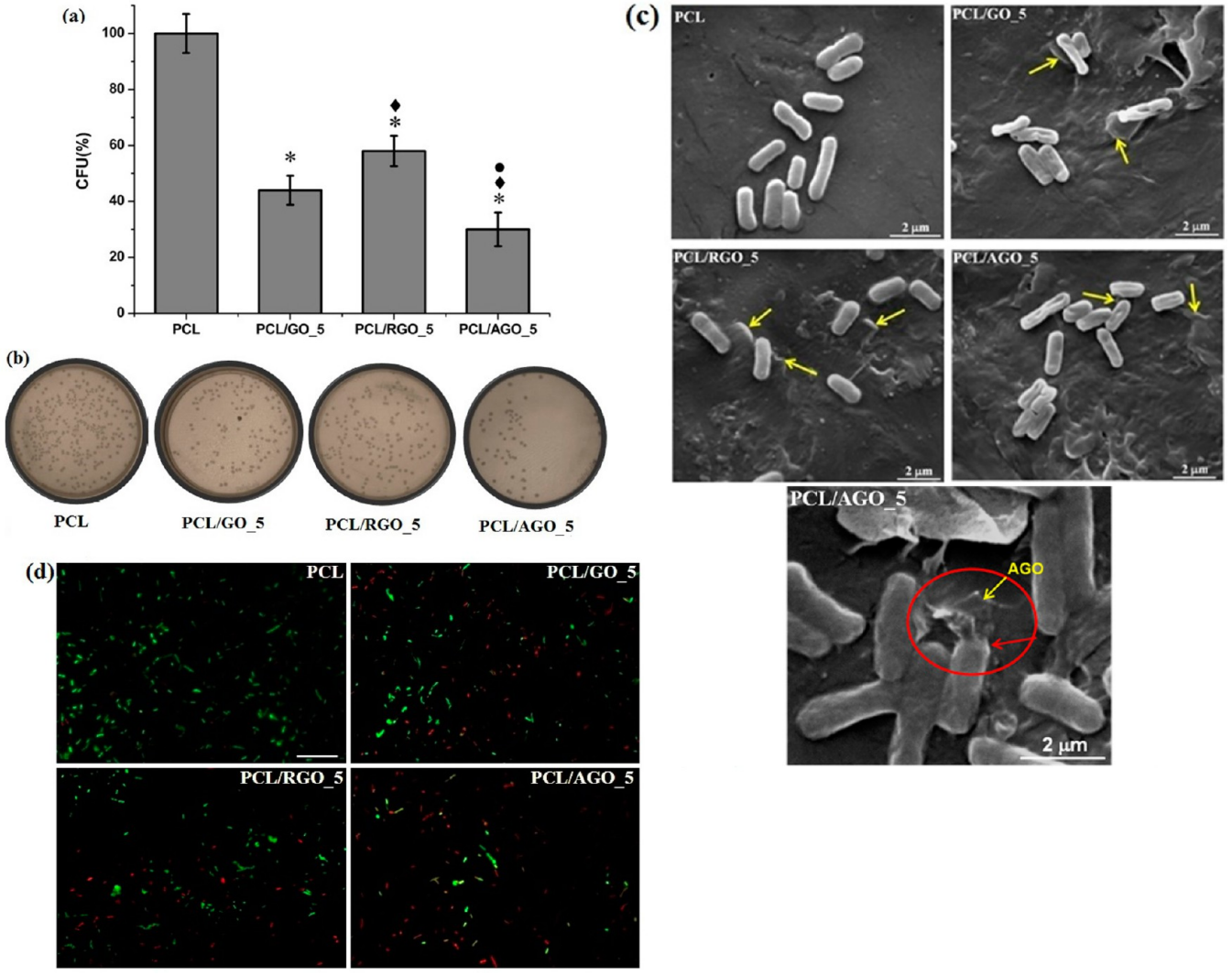

Figure 8. Bactericidal study on PCL and its different graphene derived composites. (a) Colony count with respect to the neat PCL. (b) Photographs of the viable bacterial colonies incubated on LB agar plates for neat PCL and its different graphene nanocomposites. (c) SEM micrographs of attached *E. coli* on neat PCL, PCL/GO_5, PCL/RGO_5, and PCL/AGO_5 composite surface, and (d) Fluorescence images of bacterial live/dead staining on PCL and its composite surface (scale bar = 20 μm). Statistically significant difference ($p < 0.05$) compared to neat PCL, PCL/GO_5 and, PCL/RGO_5 are indicated by *, ♦, and ●, respectively.

Figures 8a present the fraction of colony count with respect to the neat polymer supported by photographs (Figure 8b) of the viable bacterial colonies incubated on LB agar plates for neat PCL and its different graphene nanocomposites. PCL/GO_5, PCL/RGO_5, and PCL/AGO_5 composites showed significantly lower colony count with respect to neat PCL. Among the composites PCL/AGO_5 showed ∼70% decrease in colony count followed by PCL/GO_5 (56%) and PCL/RGO_5 (42%). SEM micrographs of *E. coli* attached to the composite surfaces showed the interaction between the graphene particles as shown by the yellow arrows and the bacteria (Figure 8c). Representative SEM micrograph at higher magnification for PCL/AGO_5 shows damaged membrane (red arrow) induced by AGO (yellow arrow) upon direct contact with the bacterium.

The viability of the bacterial cells adhered to the surfaces was assessed by live/dead staining. In this technique, viable cells on disc surface with intact membrane appeared green, whereas cells with damaged membrane appear red. Most of the *E. coli* adhered to the PCL surface survived as indicated by the green color (Figure 8d) indicating that their cell membrane integrity was not affected. However, most of cells on the different graphene composites appeared red due to membrane damage caused by graphene nanoparticles. Among the composites, the largest fraction of dead cells was found on PCL/AGO_5 composite surface followed by PCL/GO_5 and last PCL/RGO_5. These results of the live/dead assay corroborate the results obtained by the colony count method.

We further assessed how the initial events of bacterial interactions with the different surfaces affected biofilm formation. SEM micrographs presented in Figure 9 revealed that all the three PCL/graphene composites (PCL/GO_5, PCL/RGO_5, and PCL/AGO_5) inhibited bacterial biofilm formation. Whereas a dense and uniform bacterial biofilm was observed on PCL surface, significantly fewer adhered bacteria were seen on the composite surfaces. Moreover, PCL showed bacterial cells in large communities on its surface (Figure 9 inset). In contrast, individually attached bacteria lacking the community structure were observed on the composites. Also, *E. coli* cells exhibited rough and damaged cell morphology on the

DOI: 10.1021/am5079732
ACS Appl. Mater. Interfaces 2015, 7, 3237−3252

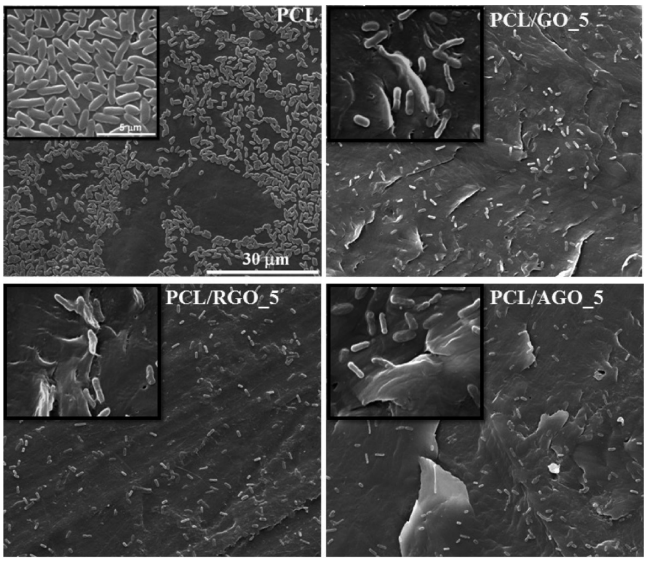

Figure 9. SEM micrographs of biofilm formation on neat PCL, PCL/GO_5, PCL/RGO_5, and PCL/AGO_5 composite surfaces.

composites surface in contrast to smooth cell morphology on neat PCL (Figure 9 inset).

The ability of a biomaterial to resist biofilm formation arises due to its ability to prevent bacterial adhesion or killing of bacteria by direct contact with the surface[64,65] PCL/graphene composites here exhibited bacterial resistance by killing of bacterial cells which came in direct contact with the graphene nanoparticles. Studies have revealed that GO kills bacteria on contact by irreversible physical rupture of the cell membrane,[66] charge transfer and formation of reactive oxygen species.[17] Presence of sharp edges and functional groups containing oxygen in GO might induce membrane damage and oxidative stress upon direct contact with bacteria on PCL/GO_5 surface.[67] Bacterial cells on PCL/AGO_5 composites showed cell damage by membrane rupture. It is believed that presence of free amine group on AGO surface impart positive charge, which facilitate binding to the negatively charged bacterial cell wall leading to membrane damage by GO nanoparticles. It has been reported that presence of primary amine or quaternary ammonium groups imparts bactericidal property to the surface arising from the damage to the bacterial membrane causing cell death.[30,68] PCL/RGO_5 composites showed slightly higher colony count in comparison to PCL/GO_5 and PCL/AGO_5 composites. RGO nanoparticles in PCL matrix thus appear to play a less effective role in improving antibacterial property. The bactericidal property of graphene derived nanoparticles primarily depends on their size and state of dispersion.[17] In general, well dispersed graphene nano sheets offer more opportunity to interact with bacterial cells in comparison to aggregated graphene sheets. Also, it has been shown that nonfunctionalized hydrophobic RGO nanoparticles when compared to functionalized GO and AGO have tendency to agglomerate due to hydrophobic interactions.[69] As a result, PCL/RGO_5 composites showed higher colony count than PCL/GO_5 and PCL/AGO_5 composites. These results suggest that PCL/AGO_5 composite exhibit the best bacterial resistance, which is likely because of the synergetic effect of chemical cues (primary amine groups and oxygenated groups) and physical cues (sharp edges of the sheet) of the functionalized AGO nanoparticles incorporated in the PCL matrix.

Table 2 summarizes the key findings of this study on the use of different chemically functionalized graphene derived nanoparticles as filler unit in PCL matrix. Mechanical studies suggested that addition of graphene improved the modulus of PCL with highest improvement observed with the use of GO nanoparticles and closely matched but lower (with statistically significant difference) for AGO. Biological studies with hMSCs showed that functionalized graphene composites (PCL/GO and PCL/AGO) better supported cell proliferation and augmented osteogenesis. Most mineralization was observed with the use of AGO followed by GO whereas RGO composite was similar to that of neat PCL. Study of biofilm formation indicated that PCL/AGO exhibited the best bactericidal property thereby resisting biofilm formation on its surface followed by PCL/GO, PCL/RGO, and last neat PCL. Taken together, AGO provides the optimal combination of improved mechanical properties, stem cell proliferation, and osteogenesis, and resistance to bacterial growth and biofilm formation. The ability of PCL/AGO surface to influence the physical, chemical and biological properties was because of presence of AGO with multifunctional chemical groups including carboxyl, hydroxyl, and amine groups on its surface. The chemical heterogeneity of AGO showed synergetic effect of chemical groups resulting in enhancing wettability, cell attachment, and proliferation because of favorable adsorption of cell-adhesive proteins by amine groups[46,49] and high mineral deposition contributing to nucleating effect of carboxyl and amine groups for calcium and phosphate ions.[57,58] The synergetic effect of amine terminated silane and methyl terminated silane on plasma coagulation response has also been reported.[24] Hence, this study elucidates the importance of different functionalization of graphene for its use in polymer composites for biomedical applications.

Table 2. Summary of Mechanical, Biological, and Antibacterial Response by Different Graphene-Derived Composites[a]

sample	rigidity	cell proliferation	stem cell osteogenesis	biofilm inhibition
PCL/GO	+++	+	+	++
PCL/RGO	+	0	0	+
PCL/AGO	++	++	++	+++

[a]Where "0" indicates no significant difference, "+" indicates a small but significant improvement, "++" indicates a larger significant improvement, and "+++" indicates the highest improvement over neat PCL.

4. CONCLUSION

PCL composites incorporating RGO, GO, and AGO of different filler contents (1%, 3%, and 5%) were fabricated to evaluate for use in orthopedic applications. Addition of the nanoparticles to PCL increased the elastic modulus. This increase was more so for GO and AGO than with RGO. Cell studies showed that presence of amine groups on AGO surface was most effective for promoting hMSC proliferation and osteogenesis. Bacterial studies revealed that although the addition of all three types of graphene imparted bactericidal property to PCL, AGO was best at inhibiting formation of biofilm. Taken together, AGO-reinforced PCL composites offer the best combination of properties for orthopedics due to the synergistic effect of oxygen containing and amine groups. This work demonstrates the key role of surface functionalization of graphene as filler in composites for biomedical applications.

DOI: 10.1021/am5079732
ACS Appl. Mater. Interfaces 2015, 7, 3237−3252

AUTHOR INFORMATION

Corresponding Author

*E-mail: kchatterjee@materials.iisc.ernet.in. Tel: +91-80-22933408.

Notes

The authors declare no competing financial interest.

ACKNOWLEDGMENTS

This work was funded by the Department of Science and Technology (DST), India. K.C. acknowledges the Ramanujan fellowship from DST. E.K. acknowledges the Department of Biotechnology, India for the Postdoctoral Research Associate fellowship. Authors gratefully acknowledge support from Prof. Shivaprasad (JNCASR) for XPS measurements, Mr. Shyam Sundar for contact angle measurements, Mr. Prasanna Kumar S. Mural for Raman and FTIR and Mr. Mohan Chokkalingam for his technical assistance with antibacterial test.

REFERENCES

(1) Rafiee, M. A.; Rafiee, J.; Wang, Z.; Song, H.; Yu, Z.-Z.; Koratkar, N. Enhanced mechanical properties of nanocomposites at low graphene content. *ACS Nano* **2009**, *3*, 3884−3890.

(2) Shahil, K. M.; Balandin, A. A. Graphene−multilayer graphene nanocomposites as highly efficient thermal interface materials. *Nano Lett.* **2012**, *12*, 861−867.

(3) Zhang, H.-B.; Zheng, W.-G.; Yan, Q.; Yang, Y.; Wang, J.-W.; Lu, Z.-H.; Ji, G.-Y.; Yu, Z.-Z. Electrically conductive polyethylene terephthalate/graphene nanocomposites prepared by melt compounding. *Polymer* **2010**, *51*, 1191−1196.

(4) Kumar, S.; Mishra, A.; Chatterjee, K. Effect of organically modified clay on mechanical properties, cytotoxicity and bactericidal properties of poly (ϵ-caprolactone) nanocomposites. *Mater. Res. Express* **2014**, *1*, 045302.

(5) Ramanathan, T.; Abdala, A.; Stankovich, S.; Dikin, D.; Herrera-Alonso, M.; Piner, R.; Adamson, D.; Schniepp, H.; Chen, X.; Ruoff, R. Functionalized graphene sheets for polymer nanocomposites. *Nat. Nanotechnol.* **2008**, *3*, 327−331.

(6) Ahamed, M.; Karns, M.; Goodson, M.; Rowe, J.; Hussain, S. M.; Schlager, J. J.; Hong, Y. DNA damage response to different surface chemistry of silver nanoparticles in mammalian cells. *Toxicol. Appl. Pharmacol.* **2008**, *233*, 404−410.

(7) Bharali, D. J.; Klejbor, I.; Stachowiak, E. K.; Dutta, P.; Roy, I.; Kaur, N.; Bergey, E. J.; Prasad, P. N.; Stachowiak, M. K. Organically modified silica nanoparticles: A nonviral vector for in vivo gene delivery and expression in the brain. *Proc. Natl. Acad. Sci. U. S. A.* **2005**, *102*, 11539−11544.

(8) Zardini, H. Z.; Amiri, A.; Shanbedi, M.; Maghrebi, M.; Baniadam, M. Enhanced antibacterial activity of amino acids-functionalized multi walled carbon nanotubes by a simple method. *Colloids Surf., B* **2012**, *92*, 196−202.

(9) Molday, R. S.; Mackenzie, D. Immunospecific ferromagnetic iron-dextran reagents for the labeling and magnetic separation of cells. *J. Immunol. Methods.* **1982**, *52*, 353−367.

(10) Sanpui, P.; Chattopadhyay, A.; Ghosh, S. S. Induction of apoptosis in cancer cells at low silver nanoparticle concentrations using chitosan nanocarrier. *ACS Appl. Mater. Interfaces.* **2011**, *3*, 218−228.

(11) Lerf, A.; He, H.; Forster, M.; Klinowski, J. Structure of graphite oxide revisited. *J. Phys. Chem. B* **1998**, *102*, 4477−4482.

(12) Park, S. Y.; Park, J.; Sim, S. H.; Sung, M. G.; Kim, K. S.; Hong, B. H.; Hong, S. Enhanced differentiation of human neural stem cells into neurons on graphene. *Adv. Mater.* **2011**, *23*, H263−H267.

(13) Bao, H.; Pan, Y.; Ping, Y.; Sahoo, N. G.; Wu, T.; Li, L.; Li, J.; Gan, L. H. Chitosan-functionalized graphene oxide as a nanocarrier for drug and gene delivery. *Small.* **2011**, *7*, 1569−1578.

(14) Shan, C.; Yang, H.; Han, D.; Zhang, Q.; Ivaska, A.; Niu, L. Water-soluble graphene covalently functionalized by biocompatible poly-L-lysine. *Langmuir.* **2009**, *25*, 12030−12033.

(15) Lee, W. C.; Lim, C. H. Y.; Shi, H.; Tang, L. A.; Wang, Y.; Lim, C. T.; Loh, K. P. Origin of enhanced stem cell growth and differentiation on graphene and graphene oxide. *ACS Nano* **2011**, *5*, 7334−7341.

(16) Hong, S. W.; Lee, J. H.; Kang, S. H.; Hwang, E. Y.; Hwang, Y.-S.; Lee, M. H.; Han, D.-W.; Park, J.-C. Enhanced neural cell adhesion and neurite outgrowth on graphene-based biomimetic substrates. *BioMed. Res. Int.* **2014**, 2014.

(17) Liu, S.; Zeng, T. H.; Hofmann, M.; Burcombe, E.; Wei, J.; Jiang, R.; Kong, J.; Chen, Y. Antibacterial activity of graphite, graphite oxide, graphene oxide, and reduced graphene oxide: Membrane and oxidative stress. *ACS Nano* **2011**, *5*, 6971−6980.

(18) Liu, Y.; Luo, Y.; Wu, J.; Wang, Y.; Yang, X.; Yang, R.; Wang, B.; Yang, J.; Zhang, N. Graphene oxide can induce in vitro and in vivo mutagenesis. *Sci. Rep.* **2013**, *3*, 3469.

(19) Depan, D.; Girase, B.; Shah, J.; Misra, R. Structure−process−property relationship of the polar graphene oxide-mediated cellular response and stimulated growth of osteoblasts on hybrid chitosan network structure nanocomposite scaffolds. *Acta Biomater.* **2011**, *7*, 3432−3445.

(20) Girase, B.; Shah, J. S.; Misra, R. D. K. Cellular mechanics of modulated osteoblasts functions in graphene oxide reinforced elastomers. *Adv. Eng. Mater.* **2012**, *14*, B101−B111.

(21) Higuchi, A.; Ling, Q.-D.; Ko, Y.-A.; Chang, Y.; Umezawa, A. Biomaterials for the feeder-free culture of human embryonic stem cells and induced pluripotent stem cells. *Chem. Rev.* **2011**, *111*, 3021−3035.

(22) McClary, K. B.; Ugarova, T.; Grainger, D. W. Modulating fibroblast adhesion, spreading, and proliferation using self-assembled monolayer films of alkylthiolates on gold. *J. Biomed. Mater. Res.* **2000**, *50*, 428−439.

(23) Ostuni, E.; Chapman, R. G.; Liang, M. N.; Meluleni, G.; Pier, G.; Ingber, D. E.; Whitesides, G. M. Self-assembled monolayers that resist the adsorption of proteins and the adhesion of bacterial and mammalian cells. *Langmuir* **2001**, *17*, 6336−6343.

(24) Miller, R.; Guo, Z.; Vogler, E. A.; Siedlecki, C. A. Plasma coagulation response to surfaces with nanoscale chemical heterogeneity. *Biomaterials* **2006**, *27*, 208−215.

(25) Bain, J. R.; Hoffman, A. S. Tissue-culture surfaces with mixtures of aminated and fluorinated functional groups. Part 2. Growth and function of transgenic rat insulinoma cells (βg i/17). *J. Biomater. Sci. Polym. Ed.* **2003**, *14*, 341−367.

(26) Woodruff, M. A.; Hutmacher, D. W. The return of a forgotten polymer—Polycaprolactone in the 21st century. *Prog. Polym. Sci.* **2010**, *35*, 1217−1256.

(27) Hummers, W. S., Jr; Offeman, R. E. Preparation of graphitic oxide. *J. Am. Chem. Soc.* **1958**, *80*, 1339−1339.

(28) Ren, P.-G.; Yan, D.-X.; Ji, X.; Chen, T.; Li, Z.-M. Temperature dependence of graphene oxide reduced by hydrazine hydrate. *Nanotechnology.* **2011**, *22*, 055705.

(29) Cao, Y.; Feng, J.; Wu, P. Polypropylene-grafted graphene oxide sheets as multifunctional compatibilizers for polyolefin-based polymer blends. *J. Mater. Chem.* **2012**, *22*, 14997−15005.

(30) Kumar, S.; Bose, S.; Chatterjee, K. Amine-functionalized multiwall carbon nanotubes impart osteoinductive and bactericidal properties in poly (ϵ-caprolactone) composites. *RSC Adv.* **2014**, *4*, 19086−19098.

(31) Perreault, F.; Tousley, M. E.; Elimelech, M. Thin-film composite polyamide membranes functionalized with biocidal graphene oxide nanosheets. *Environ. Sci. Technol. Lett.* **2013**, *1*, 71−76.

(32) Zhang, Y.; Ali, S. F.; Dervishi, E.; Xu, Y.; Li, Z.; Casciano, D.; Biris, A. S. Cytotoxicity effects of graphene and single-wall carbon nanotubes in neural phaeochromocytoma-derived pc12 cells. *ACS Nano* **2010**, *4*, 3181−3186.

(33) Hsiao, M.-C.; Liao, S.-H.; Yen, M.-Y.; Liu, P.-I.; Pu, N.-W.; Wang, C.-A.; Ma, C.-C. M. Preparation of covalently functionalized graphene using residual oxygen-containing functional groups. *ACS Appl. Mater. Interfaces.* **2010**, *2*, 3092−3099.

DOI: 10.1021/am5079732
ACS Appl. Mater. Interfaces 2015, 7, 3237−3252

(34) Guo, Y.; Sun, X.; Liu, Y.; Wang, W.; Qiu, H.; Gao, J. One pot preparation of reduced graphene oxide (RGO) or Au (Ag) nanoparticle−RGO hybrids using chitosan as a reducing and stabilizing agent and their use in methanol electrooxidation. *Carbon* **2012**, *50*, 2513−2523.
(35) Yu, G.; Wu, P. Effect of chemically modified graphene oxide on the phase separation behaviour and properties of an epoxy/polyetherimide binary system. *Polym. Chem.* **2013**, *5*, 96−104.
(36) Pan, S.; Aksay, I. A. Factors controlling the size of graphene oxide sheets produced via the graphite oxide route. *ACS Nano* **2011**, *5*, 4073−4083.
(37) Zhu, Y.; Stoller, M. D.; Cai, W.; Velamakanni, A.; Piner, R. D.; Chen, D.; Ruoff, R. S. Exfoliation of graphite oxide in propylene carbonate and thermal reduction of the resulting graphene oxide platelets. *ACS Nano* **2010**, *4*, 1227−1233.
(38) Kudin, K. N.; Ozbas, B.; Schniepp, H. C.; Prud'Homme, R. K.; Aksay, I. A.; Car, R. Raman spectra of graphite oxide and functionalized graphene sheets. *Nano Lett.* **2008**, *8*, 36−41.
(39) Ferrari, A.; Meyer, J.; Scardaci, V.; Casiraghi, C.; Lazzeri, M.; Mauri, F.; Piscanec, S.; Jiang, D.; Novoselov, K.; Roth, S. Raman spectrum of graphene and graphene layers. *Phys. Rev. Lett.* **2006**, *97*, 187401.
(40) Stankovich, S.; Dikin, D. A.; Piner, R. D.; Kohlhaas, K. A.; Kleinhammes, A.; Jia, Y.; Wu, Y.; Nguyen, S. T.; Ruoff, R. S. Synthesis of graphene-based nanosheets via chemical reduction of exfoliated graphite oxide. *Carbon.* **2007**, *45*, 1558−1565.
(41) Singh, S. K.; Singh, M. K.; Kulkarni, P. P.; Sonkar, V. K.; Grácio, J. J.; Dash, D. Amine-modified graphene: Thrombo-protective safer alternative to graphene oxide for biomedical applications. *ACS Nano* **2012**, *6*, 2731−2740.
(42) Wu, T. M.; Chen, E. C. Crystallization behavior of poly (ε-caprolactone)/multiwalled carbon nanotube composites. *J. Polym. Sci., Part B: Polym. Phys.* **2006**, *44*, 598−606.
(43) Wang, S.; Zhang, Y.; Abidi, N.; Cabrales, L. Wettability and surface free energy of graphene films. *Langmuir* **2009**, *25*, 11078−11081.
(44) Gong, L.; Kinloch, I. A.; Young, R. J.; Riaz, I.; Jalil, R.; Novoselov, K. S. Interfacial stress transfer in a graphene monolayer nanocomposite. *Adv. Mater.* **2010**, *22*, 2694−2697.
(45) Kim, H.; Abdala, A. A.; Macosko, C. W. Graphene/polymer nanocomposites. *Macromolecules.* **2010**, *43*, 6515−6530.
(46) Webb, K.; Hlady, V.; Tresco, P. A. Relationships among cell attachment, spreading, cytoskeletal organization, and migration rate for anchorage-dependent cells on model surfaces. *J. Biomed. Mater. Res.* **2000**, *49*, 362.
(47) Webb, K.; Hlady, V.; Tresco, P. A. Relative importance of surface wettability and charged functional groups on NIH 3T3 fibroblast attachment, spreading, and cytoskeletal organization. *J. Biomed. Mater. Res.* **1998**, *41*, 422.
(48) Wilson, C. J.; Clegg, R. E.; Leavesley, D. I.; Pearcy, M. J. Mediation of biomaterial−cell interactions by adsorbed proteins: A review. *Tissue Eng.* **2005**, *11*, 1−18.
(49) Ko, Y.-M.; Lee, K.; Kim, B.-H. Effect of functional groups on biodegradation and pre-osteoblastic cell response on the plasma-polymerized magnesium surface. *Jpn. J. Appl. Phys.* **2013**, *52*, 01AE01.
(50) Folkman, J.; Moscona, A. Role of cell shape in growth control. *Nature* **1978**, *273*, 345−349.
(51) Kumar, G.; Tison, C. K.; Chatterjee, K.; Pine, P. S.; McDaniel, J. H.; Salit, M. L.; Young, M. F.; Simon, C. G., Jr. The determination of stem cell fate by 3d scaffold structures through the control of cell shape. *Biomaterials.* **2011**, *32*, 9188−9196.
(52) Schakenraad, J.; Busscher, H.; Wildevuur, C. R.; Arends, J. The influence of substratum surface free energy on growth and spreading of human fibroblasts in the presence and absence of serum proteins. *J. Biomed. Mater. Res.* **1986**, *20*, 773−784.
(53) Keselowsky, B. G.; Collard, D. M.; García, A. J. Surface chemistry modulates fibronectin conformation and directs integrin binding and specificity to control cell adhesion. *J. Biomed. Mater. Res., Part A* **2003**, *66*, 247−259.
(54) Keselowsky, B. G.; Collard, D. M.; García, A. J. Integrin binding specificity regulates biomaterial surface chemistry effects on cell differentiation. *Proc. Natl. Acad. Sci. U. S. A.* **2005**, *102*, 5953−5957.
(55) Nitya, G.; Nair, G. T.; Mony, U.; Chennazhi, K. P.; Nair, S. V. In vitro evaluation of electrospun pcl/nanoclay composite scaffold for bone tissue engineering. *J. Mater. Sci.: Mater. Med.* **2012**, *23*, 1749−1761.
(56) Gaharwar, A. K.; Mihaila, S. M.; Swami, A.; Patel, A.; Sant, S.; Reis, R. L.; Marques, A. P.; Gomes, M. E.; Khademhosseini, A. Bioactive silicate nanoplatelets for osteogenic differentiation of human mesenchymal stem cells. *Adv. Mater.* **2013**, *25*, 3329−3336.
(57) Li, J.; Chen, Y.; Yin, Y.; Yao, F.; Yao, K. Modulation of nano-hydroxyapatite size via formation on chitosan−gelatin network film in situ. *Biomaterials.* **2007**, *28*, 781−790.
(58) Landis, W. J.; Jacquet, R. Association of calcium and phosphate ions with collagen in the mineralization of vertebrate tissues. *Calcif. Tissue Int.* **2013**, *93*, 329−337.
(59) Qian, L.; Zhang, H. Green synthesis of chitosan-based nanofibers and their applications. *Green Chem.* **2010**, *12*, 1207−1214.
(60) An, Y. H.; Friedman, R. J. Concise review of mechanisms of bacterial adhesion to biomaterial surfaces. *J. Biomed. Mater. Res.* **1998**, *43*, 338−348.
(61) Sousa, C.; Teixeira, P.; Oliveira, R. Influence of surface properties on the adhesion of staphylococcus epidermidis to acrylic and silicone. *Int. J. Biomater.* **2009**, *2009*, 718017.
(62) Darouiche, R.; Landon, G.; Patti, J.; Nguyen, L.; Fernau, R.; McDevitt, D.; Greene, C.; Foster, T.; Klima, M. Role of *Staphylococcus aureus* surface adhesins in orthopaedic device infections: Are results model-dependent? *J. Med. Microbiol.* **1997**, *46*, 75−79.
(63) Montanaro, L.; Campoccia, D.; Arciola, C. R. Advancements in molecular epidemiology of implant infections and future perspectives. *Biomaterials* **2007**, *28*, 5155−5168.
(64) Cheng, G.; Zhang, Z.; Chen, S.; Bryers, J. D.; Jiang, S. Inhibition of bacterial adhesion and biofilm formation on zwitterionic surfaces. *Biomaterials.* **2007**, *28*, 4192−4199.
(65) Tiller, J. C.; Liao, C.-J.; Lewis, K.; Klibanov, A. M. Designing surfaces that kill bacteria on contact. *Proc. Natl. Acad. Sci. U. S. A.* **2001**, *98*, 5981−5985.
(66) Tu, Y.; Lv, M.; Xiu, P.; Huynh, T.; Zhang, M.; Castelli, M.; Liu, Z.; Huang, Q.; Fan, C.; Fang, H. Destructive extraction of phospholipids from escherichia coli membranes by graphene nanosheets. *Nat. Nanotechnol.* **2013**, *8*, 594−601.
(67) Zhou, H.; Liu, Y.; Chi, W.; Yu, C.; Yu, Y. Preparation and antibacterial properties of Ag@ polydopamine/graphene oxide sheet nanocomposite. *Appl. Surf. Sci.* **2013**, *282*, 181−185.
(68) Isquith, A.; Abbott, E.; Walters, P. Surface-bonded antimicrobial activity of an organosilicon quaternary ammonium chloride. *Appl. Microbiol.* **1972**, *24*, 859−863.
(69) Kuila, T.; Bose, S.; Mishra, A. K.; Khanra, P.; Kim, N. H.; Lee, J. H. Chemical functionalization of graphene and its applications. *Prog. Mater. Sci.* **2012**, *57*, 1061−1105.

DOI: 10.1021/am5079732
ACS Appl. Mater. Interfaces 2015, 7, 3237−3252